Journal of Quantitative Spectroscopy & Radiative Transfer 245 (2020) 106868

Contents lists available at ScienceDirect

Journal of Quantitative Spectroscopy & Radiative Transfer

journal homepage: www.elsevier.com/locate/jqsrt

Spectral determination of μ_a, μ_s and g from single and multiple scattering signals with one optically thick sample

Peng Tian[a,b,c], Stephen M. Mutisya[b], Jiahong Jin[a,b,c], Shuai Zheng[a], Jun Q. Lu[a,b], Xin-Hua Hu[a,b,*]

[a] Institute for Advanced Optics, Hunan Institute of Science and Technology, Yueyang, Hunan 414006, China
[b] Department of Physics, East Carolina University, Greenville, NC 27858, USA
[c] School of Physics & Electronics, Hunan Institute of Science and Technology, Yueyang, Hunan 414006, China

ARTICLE INFO

Article history:
Received 6 November 2019
Revised 27 January 2020
Accepted 27 January 2020
Available online 28 January 2020

Keywords:
Turbidity
Light scattering
Radiative transfer
Inverse problems
Spectrophotometry

ABSTRACT

Development of robust and easy-to-implement methods for quantitative turbidity characterization by inherent properties of absorption and scattering can have wide applications. We report a new method for multiparameter characterization of turbid samples with three photodiodes based on the radiative transfer (RT) theory. Instead of acquiring collimated transmittance by spatial filtering and scattered light signals by integrating spheres, the method determines RT parameters from forward transmittance dominated by light of single scattering and non-hemispherical diffuse reflectance and transmittance dominated by light of multiple scattering. A Monte Carlo based inverse algorithm has been developed to rapidly obtain absorption coefficient μ_a, scattering coefficient μ_s and anisotropy factor g at multiple wavelengths. The method has been validated with different sphere suspensions against the Mie theory. RT parameters for suspensions of spheres of 0.966 μm and 11 μm in nominal diameter values has been determined in a spectral region of 460–1000 nm and the uniqueness of the inverse solutions has been proved at selected wavelengths.

1. Introduction

Spectral characterization of turbid samples by the radiative transfer (RT) theory provides powerful tools for material analysis, biomedical research, atmospheric science and other fields. Existing spectrophotometers, however, determine only the attenuation coefficient μ_t from collimated transmittance T_c measured with negligible scatter by Beer-Lambert law. Despite intense efforts over the last few decades, complex configuration and procedures of measurement must be employed in laboratory settings for spectral determination of parameters defined by the RT theory [1–6]. For these studies, T_c is measured for μ_t followed by acquiring diffused light signals dominated by multiple scattering to retrieve the absorption coefficient μ_a, scattering coefficient μ_s and anisotropy factor g as functions of wavelength λ. The latter step is completed by solving the inverse problems defined by the following stationary and source-free RT equation [7]

$$\mathbf{s}\cdot\nabla L(\mathbf{r},\mathbf{s}) = -\mu_t L(\mathbf{r},\mathbf{s}) + \mu_s \int_{4\pi} p(\mathbf{s},\mathbf{s}')L(\mathbf{r},\mathbf{s}')d\omega', \quad (1)$$

where L(**r, s**) is radiance at an intra-sample location **r** along a unit vector **s**, $\mu_t = \mu_a+\mu_s$, p(**s, s'**) is the scattering phase function for light scattered from **s'** into **s** and the integral is over all directions of scattered light. Radiance L arises from an incident beam and g is the mean value of $\cos\theta = \boldsymbol{s}\bullet\boldsymbol{s}'$ weighted by p(**s, s'**). In nearly all cases, the forward RT problems are solved by algorithms such as the methods of multiflux [8], adding-doubling [1] or Monte Carlo [2] to calculate hemispherical diffuse reflectance R_d and transmittance T_d with μ_t determined from T_c. These numerical methods have the advantage of algorithm simplicity and low computational cost even in the case of the Monte Carlo method due to hemispherical sampling of scattered light for R_d and T_d. The hemispherical R_d and T_d, however, have to be measured with one or two integrating spheres for comparison to calculated signals for solving the inverse RT problems [6]. Two major disadvantages prevent translation of this approach out of laboratories. First, determining μ_t needs samples of modest optical thickness, typically less than 6, to measure T_c which may lead to sample preparation difficulty and thickness measurement error for highly turbid samples [2]. Second, use of integrating spheres severely limits the accessibility of this approach due to time-consuming sample assembly, necessity of user training and system maintenance. It is consequently imperative that new methods are developed to determine RT parameters

* Corresponding author at: Department of Physics, East Carolina University, Greenville, NC 27858, U.S.A.
E-mail address: hux@ecu.edu (X.-H. Hu).

https://doi.org/10.1016/j.jqsrt.2020.106868
0022-4073/

by "plug-and-play" designs of signal acquisition without integrating spheres and accurate modeling of the measured signals.

For an unknown sample, no *a priori* information exists on p(**s, s'**) defined in Eq. (1) and angular details are very expensive to measure. To alleviate the difficulty using small number of detectors, an axial symmetric and a single-parameter function $p_{HG}(\cos\theta)$ proposed by Henyey and Greenstein is often adopted to approximate p(**s, s'**) in signal calculation [9]. Furthermore, scattering signal acquisition should include proper angular integration so that a smooth function like $p_{HG}(\cos\theta)$ can be used as a window averaged version of p(**s, s'**) [10]. Additionally, accurate account of the boundary conditions in signal calculation is essential to ensure the well-posedness of inverse RT problems, which include those related to light incident upon the entrance boundary and transferring to all interfaces for subsequent escape to traps or acquisition by detectors. One therefore must incorporate accurately the locations, shapes and sizes of sample, holder and detectors to handle light transport at various interfaces based on the Fresnel's equations [11]. Finally, scalable implementation of forward modeling needs to be available so that inverse solutions at multiple wavelengths can be completed rapidly or even in real time. Once these problems are solved, spectral determination of μ_a, μ_s and g from measured signals can be realized with high stability and accessibility similar to measurements by existing spectrophotometers. In addition, signals measured directly from the sample without hemispherical integration requires proper design of sample-detector configuration to eliminate contributions from light scattered from non-sample surfaces such as those of other detectors and optics near the sample assembly if they are not accounted for in modeling. This is a unique challenge in comparison to signal measurement with integrating spheres which confine nearly all scattered light inside the spheres and shield detectors from light exiting the spheres.

Previously, we reported a method for obtaining μ_t, single-scattering albedo $a = \mu_s/\mu_t$ and g without integrating spheres [5]. But it still takes two steps of μ_t determined from T_c followed by a and g extracted from non-hemispherical R_d and T_d. Here we present a new and novel method using only one sample to obtain μ_a, μ_s and g from three measured signals of non-hemispherical R_d, T_d and forward transmittance T_f. Since T_f is dominated by single-scattering light, replacing T_c by T_f not only allows optically thick turbid samples but also complements R_d and T_d that are dominated by the multiple-scattering light to improve stability of inverse solutions. With detectors placed close to the sample assembly, multiple-scattering signals detected by non-hemispherical R_d and T_d were integrated over sufficiently large solid angles to enable employment of $p_{HG}(\cos\theta)$ as the default phase function. The uniqueness of the RT parameters retrieved from measured signals has been proved with different sphere suspension samples.

2. Materials and methods

A tunable light source was used to produce an incident beam for sample measurement, which consists of a 175 W xenon source (XL1-175-A, WavMed Technologies Corp.) and an in-house built monochromator of Czerny–Turner design. A reflective diffraction grating of 1200 lines/mm (GR1205, Thorlabs) was used as the dispersive element. The incident beam has a half-maximum bandwidth about 4.7 nm for high beam intensity and divergence minimized to half-angles of 1.3° and 0.21° along the major and minor axis of a cylindrically shaped profile. The beam was further modulated at a frequency f_0 = 385 Hz with a chopper (SR540, Stanford Research Systems) and its major and minor diameters on the sample of 14.3 mm in diameter were set to 10.4 and 4.2 mm respectively with an iris. Four photodiodes of D_1–D_4 (FDS100, Thorlabs) were employed to measure indent beam intensity I_0 and scattered light intensities of I_{Rd}, I_{Td} and I_{Tf}. Each of D_2–D_4 near

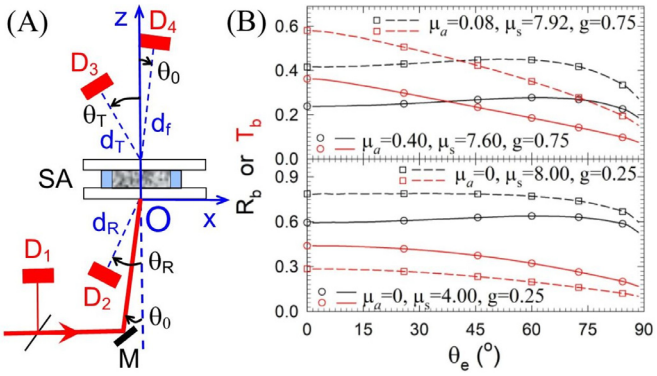

Fig. 1. (A) Sample-detector configuration: SA=sample assembly, *M*=mirror, θ_0=incident angle, θ_R and d_R (θ_T and d_T)=angle and distance of D_2 (D_3) for R_d (T_d), d_f=distance of D_4 for T_f; (B) functions of R_b (black) and T_b (red) versus θ_e for a homogeneous slab phantom for RT parameters marked. The lines are values obtained by the iMC code and symbols are those of Tables 35 and 37 in Ref. [7].

the sample assembly were installed at the end of black plastic shielding tubes so these detectors' field-of-view were limited to the front or back surfaces of the sample. It has been found experimentally that these shield tubes are critical to reduce noise background due to light scattered from other detectors and sample holder. The photodiode outputs were sampled by a 4-channel lock-in board controlled with a computer. Three measured signals were obtained as $R_d = I_{Rd}/I_0$, $T_d = I_{Td}/I_0$ and $T_f = I_{Tf}/I_0$ at each λ. As shown in Fig. 1(A), the basic acquisition configuration was designed with d_R = 21.5 mm and θ_R = 45° for D_2 measuring R_d and d_T = 35.7 mm and θ_T = 48° for D_3 measuring T_d. The D_4 detector was placed along the collimated transmission direction at a larger distance of d_f ranging from 50 to 90 mm so that the T_f signal is on the same scale as R_d and T_d signals, which can ensure the convergence of inverse calculations. The solid angles for the Rd and Td signals acquisition thus are in a range of 0.01–0.03 sr that are similar to our earlier experimental system [5]. For different samples, the above configuration was optimized slightly to increase signal-to-noise ration and avoid detector saturation. The same configuration of the sample assembly and detectors was implemented in our forward modeling to obtain calculated signals as described below.

For this study, we have prepared multiple water based sphere suspensions with different values of nominal diameter d and coefficient of variation CV. Each sample was prepared by injecting the sphere suspension into a ring spacer on an optically smooth glass slab and covered with another slab slowly to remove all air bubbles. After preparation the sample was examined under microscope to ensure very homogeneous appearance like milk with no bubbles left and optically smooth interfaces between suspension and glass slabs. The signal acquisition was performed in steps of 20 nm between 460 and 1000 nm of λ for each sample and repeated three times to determine the mean and standard deviation values. We have also measured the number concentration ρ for each sphere suspension by the masses of suspension and dry sphere component using an evaporation method [12]. For the two samples reported here, the sample thickness D and concentration ρ were measured respectively to be 0.91 ± 0.01 mm and (5.37 ± 0.02)x10^6 mm^{-3} for the sample of d = 0.966 μm and 2.10 ± 0.01 mm and (3.05 ± 0.02)x10^4 mm^{-3} for the sample of d = 11 μm. The front and back slabs of the sample holder as illustrated in Fig. 1(A) were cut from microscope slides with thickness around 1.0 mm. For validation, a Mie code [9] was used to calculate the Mueller matrix elements S_{ij} with i, j= = 1, …, 4 for a single polystyrene sphere of n_s as complex refractive index (RI)

and d as sphere diameter in a host medium water of n_w as RI for different values of λ [9]. The element S_{11} was normalized as the differential scattering cross-section to obtain the total absorption cross-section $\sigma_a(\lambda)$, total scattering cross-section $\sigma_s(\lambda)$ and anisotropy factor g(λ) of single spheres. With $n_s(\lambda)$ and $n_w(\lambda)$ retrieved from [12,13], the Mie based RT parameters for each suspension sample were derived by $\mu_{am}(\lambda) = \rho\sigma_a(\lambda)$, $\mu_{sm}(\lambda) = \rho\sigma_s(\lambda)$ and $g_m(\lambda)$ with no adjustable parameters. We note that the imaginary part n_{si} of n_s ($=n_{sr}+in_{si}$) determined from measured R_d and T_d with an integrating sphere has much larger relative measurement uncertainty than that of n_{sr} in the wavelength range of 500–1000 nm due to the extremely weak absorption. This can lead to much larger differences between $\mu_{am}(\lambda)$ by Mie and $\mu_a(\lambda)$ by the new method than those between $\mu_{sm}(\lambda)$ and $\mu_s(\lambda)$.

The RT parameters were inversely determined from the measured signals of R_d, T_d and T_f for each sample. A Monte Carlo code to track individual photons (iMC) has been developed as the forward model to calculate signals. The iMC code treats the light transport in a sample-detector configuration same as the experimental one depicted in Fig. 1(A) with algorithm details given elsewhere [2,4,14]. Briefly, N_0 photons are deposited at the front glass slab of sample assembly to represent the incident beam profile, divergence and incident angle of θ_0 set at measured values. Once into the sample, each photon is tracked as a random-walk process with free pathlengths determined by μ_s and scattering directions by $p_{HG}(\cos\theta)$ combined with random numbers (RNs). A tracked photon becomes absorbed in the sample when the cumulated free pathlength exceeds a total pathlength pre-determined by μ_a and RN. Photon interaction with sample-holder and holder-air interfaces are treated with Fresnel's equations and RNs. Once leaving the sample assembly, a photon either hits a detector being counted as a detected photon or escapes counted as a lost one. After tracking of all deposited photons, the total number of detected photons given by N_2 or N_3 or N_4 for each detector labelled in Fig. 1(A) is divided by N_0 to obtain respectively the calculated signals of non-hemispherical R_{dc} or T_{dc} or T_{fc}. To verify the iMC code, we have determined the angular dependence of injected photons leaving a semi-infinite slab sample to obtain the bidirectional curves of reflection R_b and transmission T_b as functions of exit angle θ_e. Fig. 1(B) show these curves with the values of RI for sample and glass holders set at $n = 1.00$. The excellent agreements validate the iMC code modified for this study.

To retrieve RT parameters, a gradient descent algorithm [14] was further improved to minimize the objective function δ defined below

$$\delta = \left(\frac{R_d - R_{dc}}{R_d}\right)^2 + \left(\frac{T_d - T_{dc}}{T_d}\right)^2 + \left(\frac{T_f - T_{fc}}{T_f}\right)^2. \quad (2)$$

Inverse solution was obtained at each λ by iteration in the space of μ_a, μ_s and g and stopped when $\delta \le \delta_{min}$. A threshold of $\delta_{min} = 8 \times 10^{-3}$ was chosen since the relative errors for the measured signals of R_d, T_d and T_f were estimated to be about 5% on average. The iteration time has been significantly reduced by GPU implementation of the iMC code on one graphic board (Tesla K20, Nvidia) for 50–80-fold speedup values relative to execution on one CPU (i7-3770, Intel). By gradually increasing the photon number N_0 from 5×10^6 to 5×10^7 for decreasing δ, the time for retrieving RT parameters was further reduced to within about 20 min on average with mean numbers of iterations around 500 at the first wavelength of 460 nm with μ_a around 0.2 mm^{-1} and μ_s around 10 mm^{-1}. The computing time per wavelength was further decreased to about 5 min or less as a result of closer initial parameter values and smaller μ_s values for longer wavelengths.

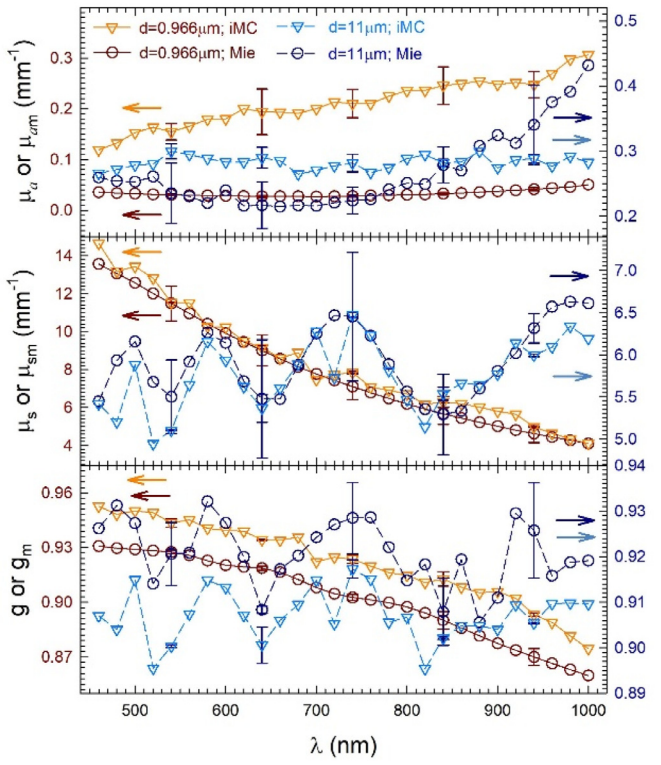

Fig. 2. Wavelength dependences of RT parameters determined by iMC and Mie theory for two sphere samples. Error bars were obtained from the standard deviations of signals by iMC simulations and CV values of sphere diameters by Mie theory. The lines are for visual guide.

3. Results

To validate the new method, we prepared suspension samples of multiple sphere types for their RT parameters with different wavelength dependence. The results of two samples are presented here with their nominal sphere diameters given respectively by $d = 0.966$ μm with CV = 1.3% (5095B, Duke Scientific) and $d = 11$ μm with CV ≤ 18% (7510B, ThermoFisher Scientific). We examined the samples under microscope and found the 0.966 μm spheres to have very uniform diameter distributions with low degree of dispersion. In contrast, the 11 μm spheres have much less uniformity with actual CV value estimated to be about 5% and visible aggregation after ultrasound treatment. In Fig. 2, we plot the RT parameters of two sphere samples determined inversely from the measured signals as functions of λ. Those obtained by the Mie theory are also presented for comparison. The distinct shapes of $\mu_s(\lambda)$ and g(λ) can be clearly observed between the two sphere types. It is particularly notable that the $\mu_s(\lambda)$ curve displays a power-law dependence for the smaller spheres whereas the larger ones present ripple structures. The former is typical of lipid emulsions such as intralipid for tissue phantoms [2,3] with nominal size parameter given by $x \le 7$ for $x = \pi d/\lambda$ and the latter is close to spherical biological cells or their nuclei [15].

The inversely determined $\mu_s(\lambda)$ curves exhibit very good agreements with Mie based $\mu_{sm}(\lambda)$ of single spheres for 0.966 μm spheres, which deteriorate at some wavelengths for 11 μm spheres. A close examination of results for the sample of 11 μm spheres indicates that disagreements are mostly in the form of $\mu_s < \mu_{sm}$, which may be attributed to the fast settling of large spheres onto the front glass slab. We found that all three measured light scattering signals were reduced by sphere aggregation after sample shaking. For a 30% decrease in T_f, for example, the settling time changes from about 30 min for 0.966 μm spheres to less than

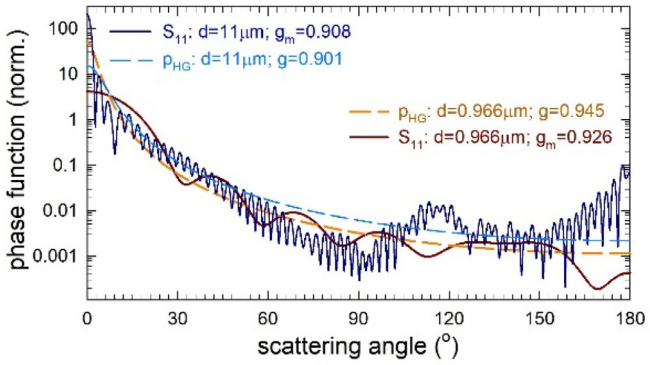

Fig. 3. Comparison of $p_{HG}(\cos\theta)$ for sphere suspensions with inversely determined g and $S_{11}(\lambda,\theta)$ of single sphere by Mie theory with g_m as the mean value of scattering angle. The λ values used in calculations are 560 nm for the 0.966 μm spheres and 640 nm for 11 μm ones.

5 min for 11 μm spheres. Consequently, the μ_s values determined from the decreased signals became underestimated relative to μ_{ms} for those wavelengths taking more than 2 min to complete data acquisition. To alleviate this problem, we manually shook larger sphere samples after each wavelength tuning but the effect cannot be totally eliminated.

In contrast, the $\mu_a(\lambda)$ curve shows quite good agreement with $\mu_{am}(\lambda)$ for the sample of 11 μm spheres while $\mu_a(\lambda)$ displays large overestimation for the sample of 0.966 μm. One needs to note that the Mie based results of μ_{sm} and μ_{am} are affected mainly by the real and imaginary RI of a sphere, n_{sr} versus n_{si}, respectively for the spectral region investigated here. Since measured values of $n_{si}(\lambda)$ have much larger uncertainty than those of $n_{sr}(\lambda)$ [12], the disagreement is expected to be larger between $\mu_a(\lambda)$ and $\mu_{am}(\lambda)$ than that between $\mu_s(\lambda)$ and $\mu_{sm}(\lambda)$. Furthermore, it is very challenging to accurately retrieve the μ_a value for samples of strong turbidity with albedo a close to 1 because of the highly "zig-zag" nature of transport within the sample for scattered light measured by detectors. This may explain the large differences between $\mu_a(\lambda)$ and $\mu_{am}(\lambda)$ for the sample of 0.966 μm spheres with a ranging from 0.988 to 0.997 and very small values of $\mu_{am}(\lambda)$. In contrast, the disagreement is much improved for the sample of 11 μm spheres which has smaller albedo values of $0.939 \le a \le 0.967$ and considerably larger $\mu_{am}(\lambda)$ values.

The widely used phase function $p_{HG}(\cos\theta)$ was employed as the default one for iMC modeling. Because of the different angular dependences between $p_{HG}(\cos\theta)$ and $S_{11}(\lambda, \theta)$, the inversely determined $g(\lambda)$ data are expected to deviate from $g_m(\lambda)$ despite their similarity in the angularly integrated wavelength dependences. Fig. 3 presents two cases of spheres at different wavelengths on angular dependences for comparing $p_{HG}(\cos\theta)$ against $S_{11}(\lambda, \theta)$. It is noticed from Fig. 2 that $g(\lambda)$ exhibits larger difference from

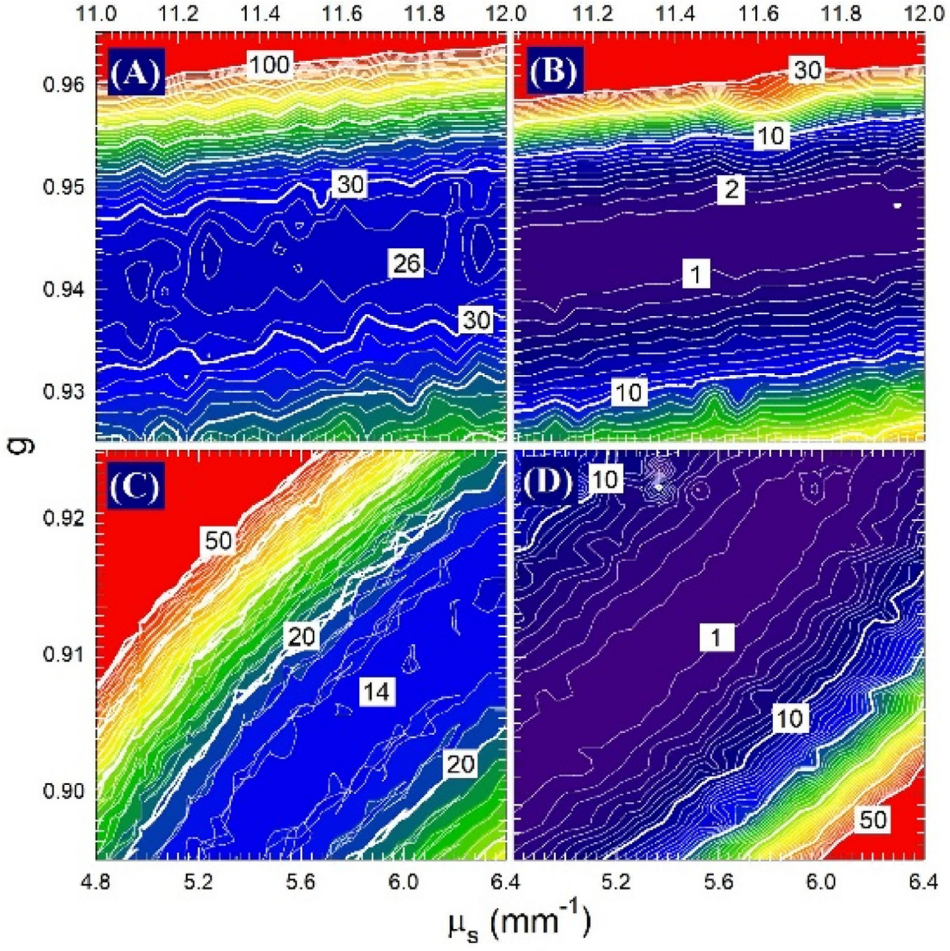

Fig. 4. Contour plots of objective function δ with values marked in% in the μ_s-g planes of different μ_a and minimum value δ_m: (A) $\mu_a = 0.100\ mm^{-1}$, $\delta_m = 23.5\%$ and (B) $\mu_a = 0.166\ mm^{-1}$, $\delta_m = 0.051\%$ for the 0.966 μm sample with signals measured at $\lambda = 560$ nm; (C) $\mu_a = 0.230\ mm^{-1}$, $\delta_m = 13.6\%$ and (D) $\mu_a = 0.289\ mm^{-1}$, $\delta_m = 0.618\%$ for the 11 μm sample at $\lambda = 640$ nm. All iMC simulations were performed with $N_0 = 1 \times 10^8$.

$g_m(\lambda)$ for the 0.966 μm spheres than those of 11 μm spheres, which can be related to a plateau of the Mie based S_{11} shown in Fig. 3 for small angles of $\theta \sim 0$ of the 0.966 μm spheres. The plateau deviates significantly from the sharply variating $p_{HG}(\cos\theta)$ and results in the larger difference in g values because of the strong forward nature of scattering. In contrast, the ripple structures in S_{11} has much reduced effect on the difference between g and g_m as evidenced in the case of 11 μm sphere. From these results, one may conclude that the single-parameter function of $p_{HG}(\cos\theta)$ provides an angularly smoothed and fairly accurate candidate for various unknown phase functions. Even with the error in the estimated g values against a "true" phase function, $p_{HG}(\cos\theta)$ can still function as a very effective tool for modeling the angular behavior of light scattering among different sample types, as illustrated in Fig. 3 for the two sphere samples.

To demonstrate the uniqueness of inverse solutions, we have calculated $\delta(\mu_a, \mu_s, g)$ in Eq. (2) at selected wavelengths for the two samples. Contour plots of $\delta(\mu_s, g)$ at two μ_a values are presented in Fig. 4 for each sample to demonstrate the variation of δ on two planes of constant μ_a. For the 0.966 μm sample, Fig. 4(B) shows $\delta(\mu_s, g)$ corresponding to the final solution of $\mu_a = 0.166\ mm^{-1}$ with minimum value $\preceq$ of δ or $\delta_m = 5.1 \times 10^{-4}$ that is much less than δ_{min}. In comparison, Fig. 4(A) displays $\delta(\mu_s, g)$ at another value of μ_a with δ_m much larger than δ_{min}. As can be seen from these results that a unique minimum exists for δ that is less then δ_{min} and thus ensure the well-posedness of the inverse solutions in this study. We further found that positioning the detectors properly from the sample assembly is important to guarantee none of the three measured signals dominating others. For example, the samples investigated here are of strong forward scattering nature. If the detector D_4, shown in Fig. 1(A) with d_f as its distance from the sample, was placed not far enough, the T_f values at different wavelengths were typically larger than those of R_d and T_d by factors of 10 or more. Inverse determination of RT parameters could exhibit instability at certain wavelengths with either δ remaining larger than δ_{min} or RT parameters exhibiting large differences from Mie based values, which can be seen in Fig. 4(A) and 4(C). For the 0.966 μm sample, the T_f values was reduced by a factor of 10^2 to be close to the values of R_d and T_d in the sale of 10^{-4} by increasing d_f from 53.5 mm to 74.9 mm with d_R and d_T kept at 21.5 and 35.7 mm, respectively. The adjustment of detector positions is very effective to improve the robustness of inverse solutions by keeping the values of measured signals on or close to the same order of magnitude.

4. Discussion

Determination of RT parameters from scattering signals measured without integrating spheres is highly desired for instrumentation development that can characterize turbidity of materials by their inherent properties. Achieving this goal is challenging and requires careful implementation of signal detection design and accurate modeling. We have validated a new method with two different sphere suspensions against the Mie theory and proved numerically the uniqueness of the inverse solutions. Additionally, the results presented in this report have demonstrated the following guidelines to meet the challenge. First, numerical modeling of signal measurement needs to be accurate in accounting for the actual arrangement of the sample, holder and detectors and has the capacity for high-performance computation. Second, the measured signals of non-hemispherical R_d and T_d are dominated by light of multiple scattering and should be sampled over sufficiently large solid angles of $\Delta\omega$, which allow the use of an angularly smooth function such as $p_{HG}(\cos\theta)$ as a substitute for the unknown phase function. We have found in this and previous studies experimentally that $\Delta\omega$ should be kept larger than 0.01 sr or 6° in polar and azimuthal angles [5]. Furthermore, these signals have to be acquired "cleanly" or with minimal contributions from light scattered by objects other than the sample to ensure modeling accuracy. Third, measurement of forward transmittance T_f yields information complementing to those produced by the angle scattering signals of R_d and T_d. For our samples with large values of optical thickness τ ($=\mu_t D$) ranging from 5 to 14 and g, T_f is dominated by light of single scattering in forward directions and thus very effective in retrieval of μ_s and g. This strategy is especially useful in measuring biological samples like cell suspensions that have g values close to 1 [16,17]. Last, adjustment of detector positions to avoid dominance of the objective function δ by one signal is very beneficial to ensure high robustness and stability of the inverse solutions on wavelengths using the RT parameters of the previous one as the initial values.

With only three photodiodes to measure light of either single or multiple scattering, the new method presented here provides a compact implementation of the above guidelines for determination of RT parameters from a turbid sample. The attractive features include the accurate and high-performance Monte Carlo modeling for signal calculation and simplicity for signal measurement. Without integrating spheres and measurement of T_c by spatial filtering, system maintenance and sample preparation are significantly simplified and optically thick samples can be accommodated. It should be noted that the measured signals of R_d and T_d are defined differently between this study and those using integrating spheres to average the scattered light over hemispherical solid angles. With integrating spheres, detector outputs are multiplied by the area ratio of sphere and detector sensor to obtain hemispherical R_d and T_d [2]. Therefore, the scattered light intensities and signal-to-noise ratios for the detector outputs are similar between the current method and previous ones. It is further observed that the measured signals of non-hemispherical R_d and T_d vary on the orders of 10^{-3}–10^{-4}. Without integrating spheres to confine the light exit from the measured sample, one has to carefully shield the detectors from the light reflected by objects surrounding the sample. Even though such requirement can be met experimentally to achieve consistency between measured and calculated signals for minimizing δ, relaxation of such stringent requirement is possible by including light scattering by surrounding objects in Monte Carlo modeling. We finally note that the gradient descent based inverse calculations by iterating Monte Carlo simulations can be significantly improved to reduce numerical variance and increase speed by deep learning neural networks trained beforehand.

Declaration of Competing Interest

The authors declare that they have no known competing financial interests or personal relationships that could have appeared to influence the work reported in this paper.

CRediT authorship contribution statement

Peng Tian: Software, Methodology, Data curation, Writing - review & editing. **Stephen M. Mutisya:** Methodology, Data curation, Writing - review & editing. **Jiahong Jin:** Software, Methodology. **Shuai Zheng:** Data curation. **Jun Q. Lu:** Software, Writing - review & editing. **Xin-Hua Hu:** Conceptualization, Methodology, Funding acquisition, Supervision, Software, Data curation, Writing - original draft.

Acknowledgment

We thank Dr. Kenneth Jacobs of Physics Department, East Carolina University for assistance in system development.

Supplementary materials

Supplementary material associated with this article can be found, in the online version, at doi:10.1016/j.jqsrt.2020.106868.

References

[1] Prahl SA, van Gemert MJC, Welch AJ. Determining the optical properties of turbid media by using the adding-doubling method. Appl Opt 1993;32:559–68.
[2] Chen C, Lu JQ, Ding H, Jacobs KM, Du Y, Hu XH. A primary method for determination of optical parameters of turbid samples and application to intralipid between 550 and 1630 nm. Opt Express 2006;14:7420–35.
[3] Aernouts B, Zamora-Rojas E, Van Beers R, Watte R, Wang L, Tsuta M, et al. Supercontinuum laser based optical characterization of Intralipid phantoms in the 500–2250 nm range. Opt Express 2013;21:32450–67.
[4] Chen X, Feng Y, Lu JQ, Liang X, Ding J, Du Y, et al. Fast method for inverse determination of optical parameters from two measured signals. Opt Lett 2013;38:2095–7.
[5] Liang X, Li M, Lu JQ, Huang C, Feng Y, Sa Y, et al. Spectrophotometric determination of turbid optical parameters without using an integrating sphere. Appl Opt 2016;55:2079–85.
[6] Lemaillet P, Cooksey CC, Hwang J, Wabnitz H, Grosenick D, Yang L, et al. Correction of an adding-doubling inversion algorithm for the measurement of the optical parameters of turbid media. Biomed Opt Express 2018;9:55–71.
[7] van de Hulst HC. Multiple light scattering: tables, formulas, and applications. New York: Academic Press; 1980.
[8] Sandoval C, Kim AD. Deriving Kubelka-Munk theory from radiative transport. J Opt Soc Am A 2014;31:628–36.
[9] Bohren CF, Huffman DR. Absorption and scattering of light by small particles. New York: Wiley; 1983. p. 65.
[10] Mourant JR, Boyer J, Hielscher AH, Bigio IJ. Influence of the scattering phase function on light transport measurements in turbid media performed with small source-detector separations. Opt Lett 1996;21:546–548.
[11] Ding H, Lu JQ, Jacobs KM, Hu XH. Determination of refractive indices of porcine skin tissues and intralipid at eight wavelengths between 325 and 1557 nm. J Opt Soc Am A 2005;22:1151–7.
[12] Ma X, Lu JQ, Brock RS, Jacobs KM, Yang P, Hu XH. Determination of complex refractive index of polystyrene microspheres from 370 to 1610 nm. Phys Med Biol 2003;48:4165–72.
[13] Hale G, Querry M. Optical constants of water in the 200 nm to 200 micrometer wavelength region. Appl Opt 1973;12:555–63.
[14] Tian P, Chen C, Jin J, Hong H, Lu JQ, Hu XH. Quantitative characterization of turbidity by radiative transfer based reflectance imaging. Biomed Opt Express 2018;9:2081–94.
[15] Wu TT, Qu JY, Xu M. Unified Mie and fractal scattering by biological cells and subcellular structures. Opt Lett 2007;32:2324–6.
[16] Lu JQ, Yang P, Hu XH. Simulations of light scattering from a biconcave red blood cell using the FDTD method. J Biomed Opt 2005;10:024022.
[17] Ding H, Lu JQ, Brock RS, McConnell TJ, Ojeda JF, Jacobs KM, et al. Angle-resolved Mueller matrix study of light scattering by B-cells at three wavelengths of 442, 633 and 850 nm. J Biomed Opt 2007;12:034032.

Journal of Quantitative Spectroscopy & Radiative Transfer 253 (2020) 107024

Contents lists available at ScienceDirect

Journal of Quantitative Spectroscopy & Radiative Transfer

journal homepage: www.elsevier.com/locate/jqsrt

Corrigendum

Corrigendum to "Spectral determination of μa, μs and g from single and multiple scattering signals with one optically thick sample" Journal of Quantitative Spectroscopy & Radiative Transfer 245 (2020) 106868

Peng Tian[a,b,c], Stephen M. Mutisya[b], Jiahong Jin[a,b,c], Shuai Zheng[a], Jun Q. Lu[a,b], Xin-Hua Hu[a,b,*]

[a] Institute for Advanced Optics, Hunan Institute of Science and Technology, Yueyang, Hunan 414006, China
[b] Department of Physics, East Carolina University, Greenville, NC 27858, USA
[c] School of Physics & Electronics, Hunan Institute of Science and Technology, Yueyang, Hunan 414006, China

The authors regret that the thickness D was erroneously reported in the published article for the sphere sample with d = 0.966 μm as nominal diameter. The correct value and estimated error of D should be given by 2.06 ± 0.01 mm, and not 0.91 ± 0.01 mm as it is printed in the third paragraph of the Materials and Methods section. We note that all other results and conclusions remain unaffected since all Monte Carlo simulations were performed with the D value as corrected here.

The authors would like to apologise for any inconvenience caused.

Declaration of Competing Interest

The authors declare that they have no known competing financial interests or personal relationships that could have appeared to influence the work reported in this paper.

DOI of original article: 10.1016/j.jqsrt.2020.106868
* Corresponding author.
E-mail address: hux@ecu.edu (X.-H. Hu).

https://doi.org/10.1016/j.jqsrt.2020.107024